Available online at www.sciencedirect.com
ScienceDirect
Trans. Nonferrous Met. Soc. China 34(2024) 519−532
Transactions of Nonferrous Metals Society of China
www.tnmsc.cn

Microstructural evolution and formability of Ti−6Al−4V alloy sheet during electropulsing-assisted bending

Ling-jian MENG[1], Hong-liang YIN[1], Yan ZHU[1], Xiao-lei CUI[2], Peng LIN[1,3]

1. College of Materials Science and Engineering, Taiyuan University of Technology, Taiyuan 030024, China;
2. National Key Laboratory for Precision Hot Processing of Metals, Harbin Institute of Technology, Harbin 150001, China;
3. Engineering Research Center of Advanced Metal Composites Forming Technology and Equipment of Ministry of Education, Taiyuan University of Technology, Taiyuan 030024, China

Received 25 July 2022; accepted 10 November 2022

Abstract: The electropulsing-assisted bending test was carried out on Ti−6Al−4V alloy sheet with the effective current density of 0−3.2 A/mm^2 and duty ratio of 10%−70%. The results show that the bending forming displacement increased from 9.15 to 15.60 mm with increasing effective current density from 0 to 2.4 A/mm^2. The crack changed to be shallow and small at the same time. Besides, the springback angle decreased as the effective current density increased at the bending displacement of 8 mm. Duty ratio also affected bending angle, where 30% duty ratio led to the lowest bending angle of 135.0°. The thermal stability temperature increased with increasing effective current density and varied non-monotonically with duty ratio. In addition, grain coarsening, {0001} texture strengthening and sub-grain development were observed during electropulsing-assisted bending. The electropulsing decreased dislocation density and accelerated dislocation rearrangement, the rearranged and piled-up dislocation inside α grains promoted sub-grain structure formation, which improved the formability. The contribution of athermal effect made the low-temperature formability of Ti−6Al−4V alloy comparable to that at high temperature.

Key words: Ti−6Al−4V alloy sheet; microstructural evolution; formability; electropulsing-assisted bending; springback; dislocation; athermal effect

1 Introduction

Titanium alloy has become an attractive lightweight structure material due to the combination of high strength, low density and good corrosion resistance [1,2]. Especially, Ti−6Al−4V alloy sheet is widely used in aerospace, marine industry, automotive and chemical industry. However, the high strength of Ti−6Al−4V alloy leads to large forming force and high deformation resistance at ambient temperature, which may cause cracking during sheet forming process. In addition, the large springback of Ti−6Al−4V alloy sheet after deformation makes the high-precision sheet forming difficult.

Conventionally, hot forming process is applied to improving the formability of lightweight alloy sheet due to the remarkable thermal effect [3−6]. ZHAN et al [3] reviewed the development of hot spinning technique for the production of light metal complex parts. Such a hot forming process extended the forming limit of materials, decreased the forming forces and reduced process chains. ZONG et al [6] investigated the springback characteristics during hot V-bending process of Ti−6Al−4V alloy sheet, and found that the positive and negative springback occurred at 300−650 °C and

Corresponding author: Peng LIN, Tel/Fax: +86-351-6010021, E-mail: linpeng@tyut.edu.cn
DOI: 10.1016/S1003-6326(23)66414-3

700−750 °C, respectively. The springback angle decreased as temperature increased. In addition, the microstructure and deformation mechanism during high temperature deformation of titanium alloy sheet have also been researched [7−9]. FAN et al [8] revealed the relationship between microstructure and mechanical properties of TA-32 titanium alloy sheets during tensile deformation at 800 °C. The grain coarsening and dislocation annihilation weakened the deformation ability of material. Although the traditional hot sheet forming technique is effective to reduce flow stress and springback, it still has shortcomings. The low thermal conductivity of titanium alloy sheet causes temperature gradient and residual stress. The oxidation and grain coarsening decrease the mechanical properties.

Compared with traditional thermal forming, electropulsing-assisted sheet forming has received much attention due to lower cost of time and energy. SHENG et al [10] reviewed the effect of high-density electropulsing treatment on microstructure and properties of metallic materials. The improved fatigue property and corrosion performance by electropulsing were attributed to grain refinement and recrystallization. AMBROGIO et al [11] proposed a hot incremental sheet forming method assisted by current, which allowed a higher formability as compared to cold forming. Some researchers also investigated the electropulsing-assisted sheet forming of Ti−6Al−4V alloy. AO et al [12] found that the increase of electropulsing parameters enhanced formability of Ti−6Al−4V alloy sheet during incremental forming, and the maximum fracture depth of groove rose to 7.0 mm, which increased by 52.2% compared with conventional ambient incremental forming. SONG et al [13] found that the electropulsing treatment significantly improved the formability of Ti−6Al−4V alloy sheet. The uniform elongation increased by 35%, the yield stress decreased by 19.8% and the ratio of yield to tensile decreased by 17.6%.

Researchers mostly agree that thermal effect and athermal electroplastic effect both contribute to the improvement of sheet formability under electropulsing. Thermal effect is the generated Joule heating when current flows through the material, whereas the athermal effect generally consists of electron wind effect, magnetic compression effect and skin effect [14,15]. AO et al [16] clarified that the athermal effect promoted dislocation motion and pile-up unraveling, therefore suppressed the springback during V-bending of Ti−6Al−4V alloy sheet. ZHAO et al [17] found that the grain growth, thermal expansion on dislocation motion, and phase transformation contributed to stress softening, which relieved the springback of Ti−6Al−4V sheets during stretch U-bending. ZHOU et al [18] studied the effect of electropulsing on deformation behavior of Ti−6Al−4V alloy during cold drawing, and found that electropulsing enhanced the deformability of the grains with unfavorable orientations by promoting prismatic $\langle a \rangle$ slip moving. However, previous researches are insufficient on the microstructure and texture of Ti−6Al−4V alloy sheet during electropulsing-assisted bending. The relationship among microstructure, temperature field and formability improvement has not been studied systematically.

In this research, the temperature field and heating behaviors of Ti−6Al−4V alloy sheet during electropulsing-assisted V-bending process were studied. The effects of electropulsing parameters on forming limit and springback behavior were revealed. The microstructure and texture evolution during bending and their effect on formability were discussed. The athermal effect of electropulsing was confirmed and discussed from the viewpoint of dislocation. This research provides an approach for improving the formability of titanium alloys at low temperatures.

2 Experimental

The chemical composition of as-received Ti−6Al−4V rolled sheet is listed in Table 1. The electropulsing-assisted V-bending platform in present study was established based on UTM4304 electronic universal testing machine. The live view and schematic diagram of experimental setup are shown in Figs. 1(a) and (b), respectively. The die and punch were insulated from the equipment, where current flowed into the specimen from the

Table 1 Chemical composition of Ti−6Al−4V alloy sheet (wt.%)

Al	V	Fe	C	H	O	Ti
5.917	4.164	0.115	0.005	0.008	0.071	Bal.

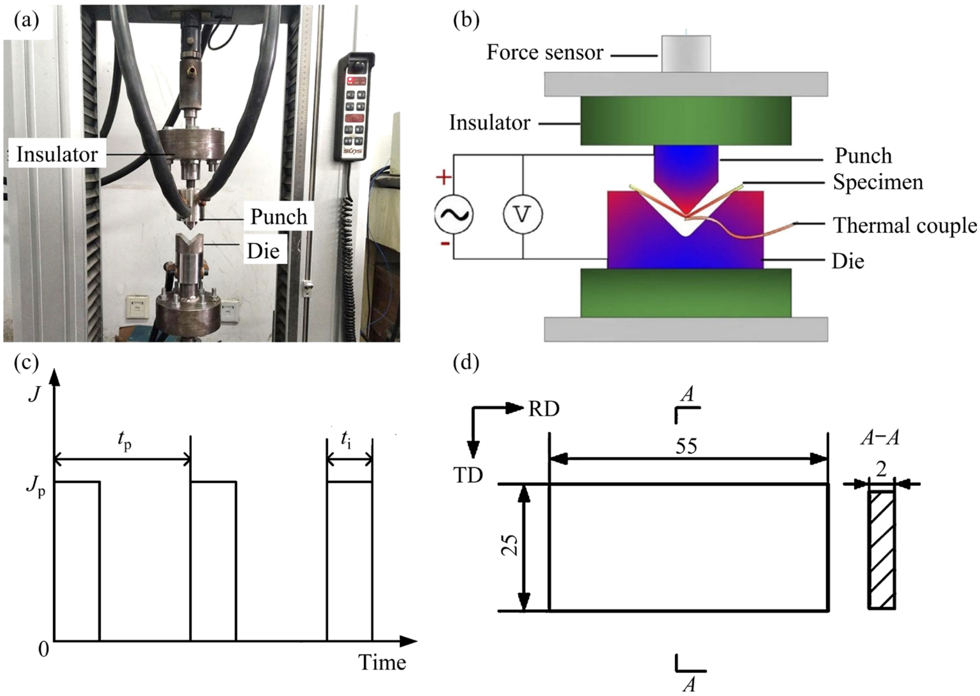

Fig. 1 Live view (a) and schematic diagram (b) of electropulsing-assisted bending platform, electropulsing waveform (c), and dimensions of bending specimen (d) (Unit: mm)

punch and flowed out through the die. K-type thermal couple was welded at different positions of specimen to obtain the temperature distribution. The pulsed current was provided by a CTNP−12/2000(6000)FN electropulsing generator with an input current of 2000 A and a maximum output current of 6000 A, where the output current can be adjusted through the current percentage (r_a). The peak current density J_p, effective current density J_e, duty ratio D_c and their relationships were described in Eqs. (1) to (3):

$$J_e = \frac{2000 r_a}{S_0} \tag{1}$$

$$J_p = J_e / D_c \tag{2}$$

$$D_c = t_i / t_p \tag{3}$$

where effective current density J_e represents the total current flowing in the alloy sheet divided by cross sectional area (S_0). As shown in the waveform schematic in Fig. 1(c), peak current density J_p is the maximum current density of electropulsing, duty ratio D_c means the ratio of power-on time (t_i) to an entire pulse period (t_p).

The as-received 2 mm-thick alloy sheet was cut into bending specimens along rolling direction with the gauge dimensions of 25 mm (width) × 55 mm (length), as shown in Fig. 1(d), where RD and TD represent the rolling direction and transverse direction, respectively. Bending test was carried out with a punch speed of 5 mm/min and a punch degree of 90°. To investigate the effect of electropulsing parameters on the bending behavior, the effective current densities were set to be 1.2, 1.6, 2.0, 2.4, 2.8 and 3.2 A/mm^2, the pulse duty ratio varied from 10% to 70%, and the pulse frequency was set to be 1000 Hz. Specimens were tested three times under each bending condition to ensure repeatability. The microstructure was characterized by optical microscope (LEICA DM2700M) and scanning electron microscope (SEM, TESCAN MIRA3 LMH) equipped with electron backscatter diffraction (EBSD). The location for microscopic characterization was at the radius corner of bended Ti−6Al−4V alloy sheet. The EBSD specimens were electrochemically polished in a solution of 6 vol.% perchloric acid, 60 vol.% butanol, and 34 vol.% carbinol for 60 s with current density of 1.0 A/cm^2 and operating voltage of 36 V.

3 Results

3.1 As-received microstructure

Figure 2(a) shows the backscattered electron (BSE) image of as-received Ti−6Al−4V alloy sheet.

The light contrast region represents β phase and dark contrast region represents remained α phase. Figure 2(b) displays the inverse pole figure (IPF) map of α phase, where β phase is ignored during EBSD analysis. The α phase exhibits the equiaxed or continuous morphology, which is distributed homogeneously in the β matrix. The grain size distribution and (0001) pole figure (PF) are shown in Figs. 2(c) and (d), respectively. The average grain size of α phase was calculated to be 4.28 μm. The α phase has a texture adjacent to (0001) orientation, where the peak pole intensity splits by ±15° from normal direction (ND).

3.2 Forming limit under electropulsing

The forming limit of Ti−6Al−4V alloy sheet was investigated under different effective current densities. As shown in the displacement−bending load curves in Fig. 3(a), the alloy sheet ruptured at the bending displacement of 9.15 mm without electropulsing, the bending displacement reaches 10.40, 13.35, 14.05, and 15.60 mm at 1.2, 1.6, 2.0, and 2.4 A/mm^2, respectively. The forming limit increases and the load value decreases as the effective current density increases. The improvement of formability by electropulsing is also observed from the crack morphologies in Fig. 3(b). The displacements of specimens in Fig. 3(b) are the same to the bending displacement after rupture in Fig. 3(a). The cracks appear at the radius corner of the alloy sheet due to the large deformation. The deep and large crack changes to be shallow and small as the effective current density increases. This is because crack hindered current flowing, leading to high current density at crack tip and low current density at the crack center. The high current density increased temperature by Joule heating effect and generated thermal stress around the crack tip, arrested the crack propagation and healed the crack [19].

The thermal effect and temperature increase are the reasons for formability improvement [5,20]. Figure 3(c) displays the temperature at different positions of alloy sheet under effective current density of 2.4 A/mm^2. The schematic diagram of temperature measurement positions is shown in the figure. Firstly, the temperature increases rapidly with increasing bending time, following a nearly liner relationship. Then, the slop of curve decreases gradually until the temperature reaches a constant value. It is not difficult to find that the temperature decreases from the radius corner (Point 1) to the outside part (Point 3), which is because the radius corner is the dominant deformation region during

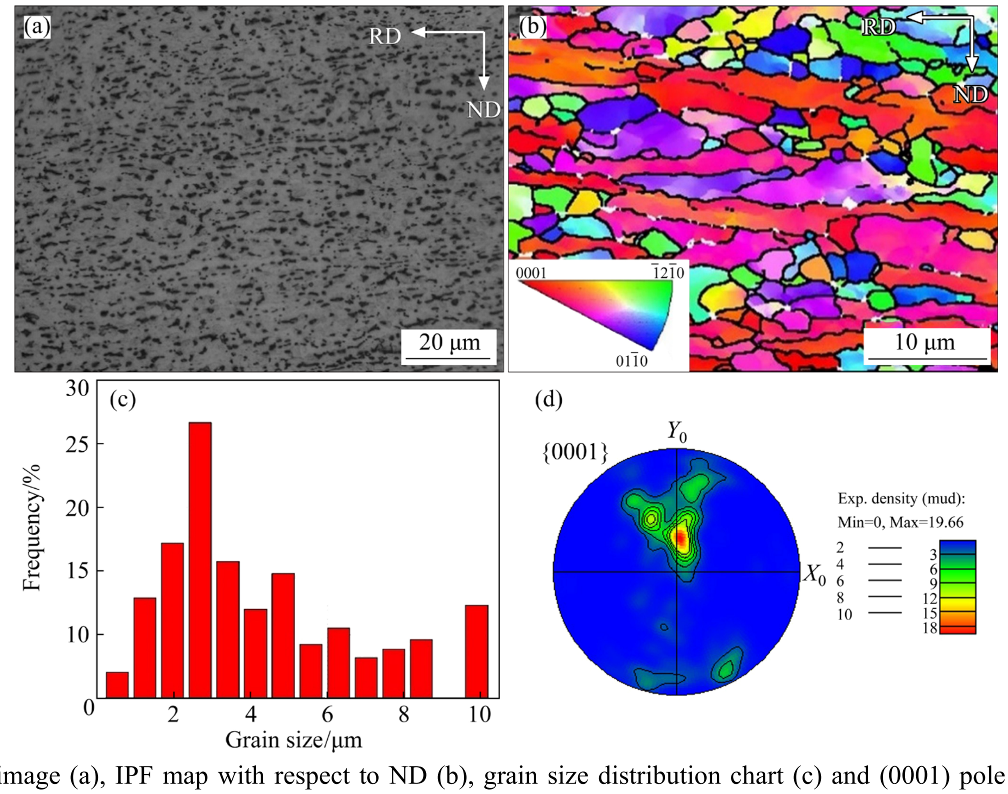

Fig. 2 BSE image (a), IPF map with respect to ND (b), grain size distribution chart (c) and (0001) pole figure (d) of as-received Ti−6Al−4V alloy sheet

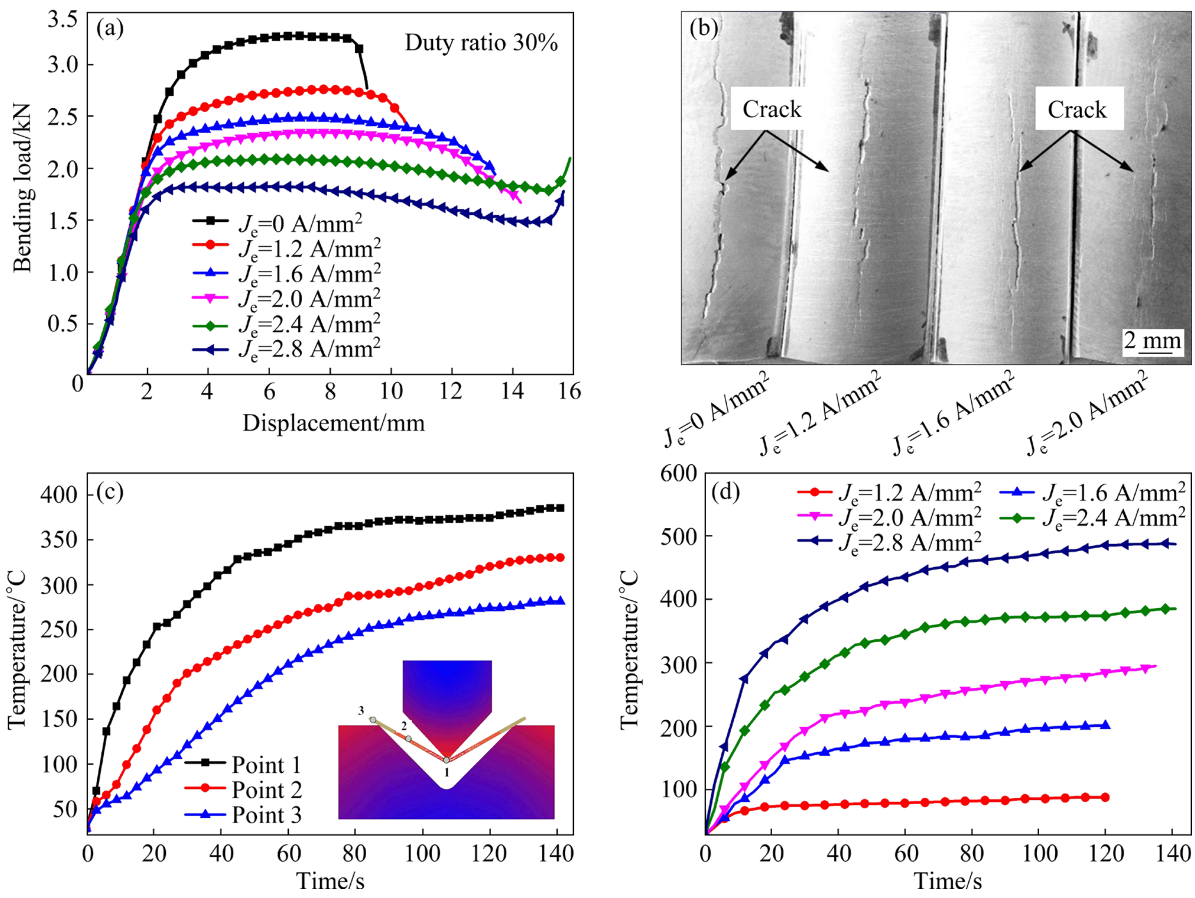

Fig. 3 Displacement−bending load curves (a) and crack morphologies at different effective current densities (b), and temperature change at different positions and 2.4 A/mm^2 (c) and at different effective current densities and Point 1 (d)

bending. The thermal stability temperatures reach 385, 330, and 281 °C at Points 1, 2, and 3, respectively. Figure 3(d) depicts the temperature change at different effective current densities. The thermal stability temperatures at Point 1 are 88, 201, 298, 385, and 487 °C under the effective current densities of 1.2, 1.6, 2.0, 2.4, and 2.8 A/mm^2, respectively. The higher effective current density caused higher heating rate and higher thermal stability temperature, therefore improved the forming limit as shown in Fig. 3(a).

3.3 Springback under electropulsing

The effect of effective current density on springback behavior was investigated with the same bending displacement of 8 mm. The displacement−bending load curves are presented in Fig. 4(a). The curves are well overlapped during elastic deformation, implying that the effective current density hardly affects elastic modulus. During plastic deformation, the bending load value decreases as the effective current density increases. The effect of effective current density on bending angle of alloy sheet is shown in Fig. 4(b). It can be observed that the bending angle decreases as effective current density increases. When the effective current density increases from 0 to 2.0 A/mm^2, the bending angle slightly changes from 149.2° to 146.3°. However, the bending angle greatly changes from 144.6° to 135.0° when the effective current density increases from 2.4 to 3.2 A/mm^2. The above results indicate that the high current density can suppress springback significantly during bending of Ti−6Al−4V alloy sheet.

In addition, the effect of duty ratio on springback was investigated with the same bending displacement of 8 mm and effective current density of 3.2 A/mm^2. As presented in Fig. 4(c), the duty ratio has limited effect on elastic modules. During plastic deformation stage, the bending loads are 2729.6, 1219.1, 2260.8, and 2473.2 N at duty ratios of 10%, 30%, 50%, and 70%, respectively. The bending load firstly decreases and then increases with the increase of duty ratio. Figure 4(d) presents the bending angles under different duty ratios. The lowest bending angle was obtained at the duty ratio of 30%, which was attributed to the low yield strength and alloy softening effect.

Figure 5 depicts the temperature at Point 1 under different effective current densities and duty ratios. The thermal stability temperature at Point 1 is only 88 °C without current, leading to a large springback as shown in Fig. 4(b). The thermal stability temperature is the highest at a current density of 3.2 A/mm^2, leading to lowest loading value and springback. The temperature varies non-monotonically with duty ratio as shown in Fig. 5(b). This is because low duty ratio represents short power-on time, and high duty ratio represents low peak current density as shown in Fig. 1(c) and Eq. (2). Therefore, 70% duty ratio did not lead to

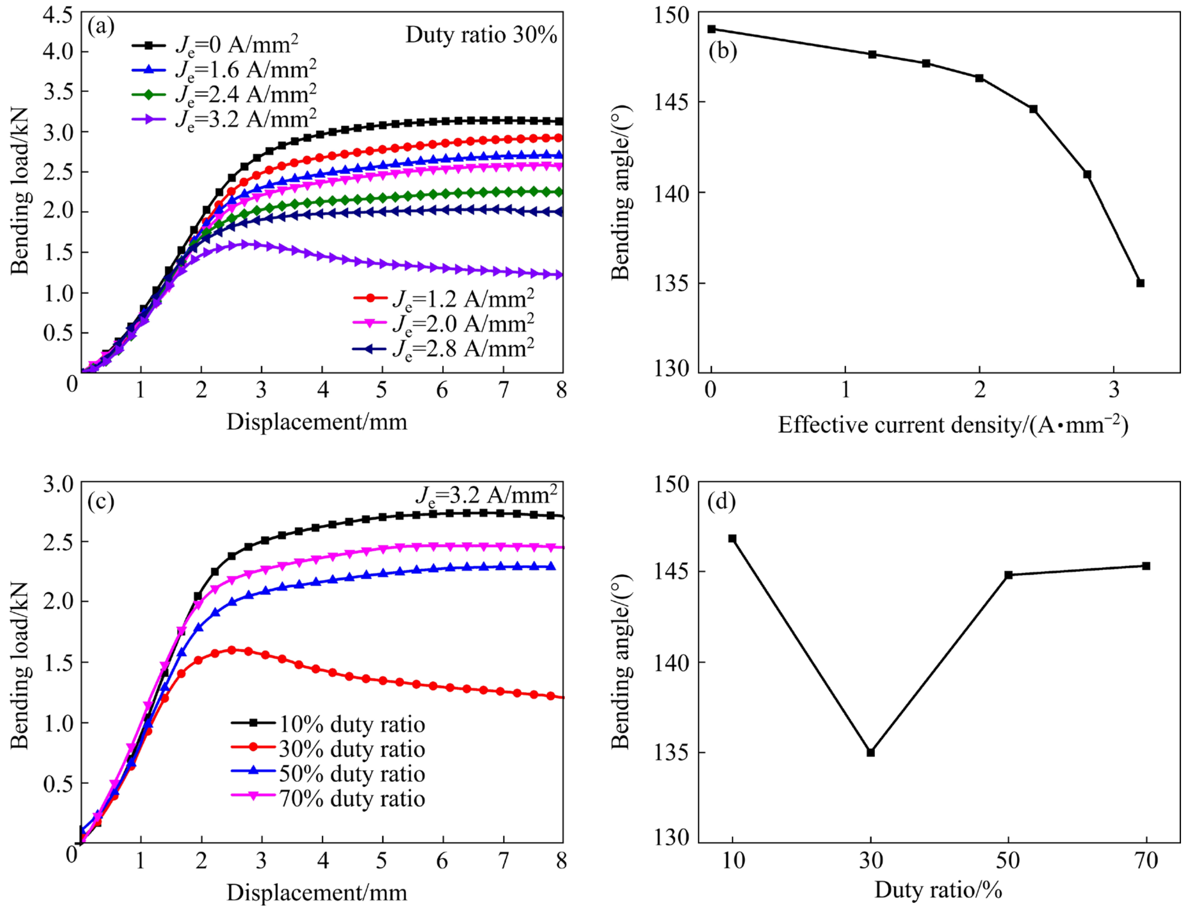

Fig. 4 Displacement−bending load curves (a, c) and bending angles (b, d) at different effective current densities (a, b) and duty ratios (c, d) and displacement of 8 mm

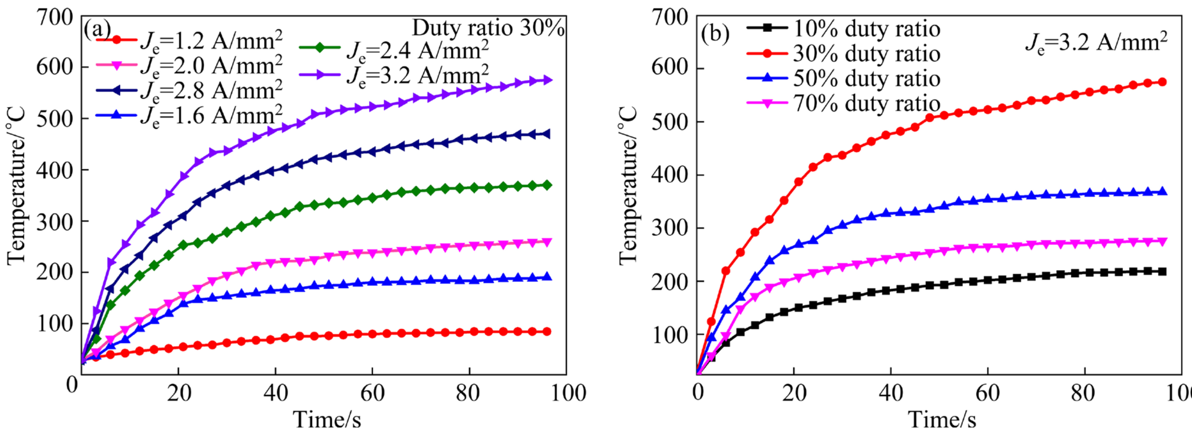

Fig. 5 Temperature dependence on effective current density (a) and duty ratio (b) at Point 1 and displacement of 8 mm

the largest thermal effect, the temperature is the highest and bending angle is the lowest at the intermediate duty ratio of 30%.

3.4 Microstructure of electropulsing-assisted bended alloy sheet

It is known that the mechanical properties and formability of titanium alloys are highly influenced by microstructure and texture. Figure 6(a) shows the microstructure at radius corner of bended Ti−6Al−4V alloy sheet without electropulsing. α grains show elongated and equiaxed morphologies after deformation. The average grain size of α phase is 4.50 μm as shown in Fig. 6(c), which is close to the grain size of as-received alloy (4.28 μm), indicating that the bending without electropulsing hardly changes the grain size of α phase. Figure 6(b) depicts the microstructure at radius corner and current density of 3.2 A/mm^2. The average grain size of α phase is 6.20 μm as shown in Fig. 6(c), which is larger than that of as-received alloy sheet. The electropulsing caused temperature increase, therefore α grain coarsening occurred [21].

Figure 6(d) shows the texture of bended specimens. The specimen without electropulsing presents a typical {0001} basal texture with the maximum density of 21.79 mud, which is similar to the as-received alloy in Fig. 2. Mud (multiple of uniform density) is the unit of texture intensity. However, the peak of pole intensity has a ±15° misorientation compared with that of the as-received alloy, implying that the cold deformation caused the grain rotation to ND. The specimen with electropulsing shows a stronger {0001} basal texture with the maximum density of 40 mud. In addition, the {0001} orientated grains become more dominant as shown in the {0001} pole figure. Thus, the electropulsing significantly promoted the {0001} texture formation during bending. This may be attributed to the prominent slip system activation and grain growth at high temperature.

Figure 7 presents grain boundary distribution maps at radius corner of bended specimen. The red line and black line represent low angle grain boundary (<15°, LAGB) and high angle grain boundary (>15°, HAGB), respectively. It is observed that the LAGB fraction is higher in the specimen with electropulsing, implying the formation of sub-grain structure. This is because deformation at ambient temperature accelerated the dislocation accumulation inside grains and suppressed the dislocation motion. On the contrary, the deformation under electropulsing at high temperature relieved the dislocation tangle and

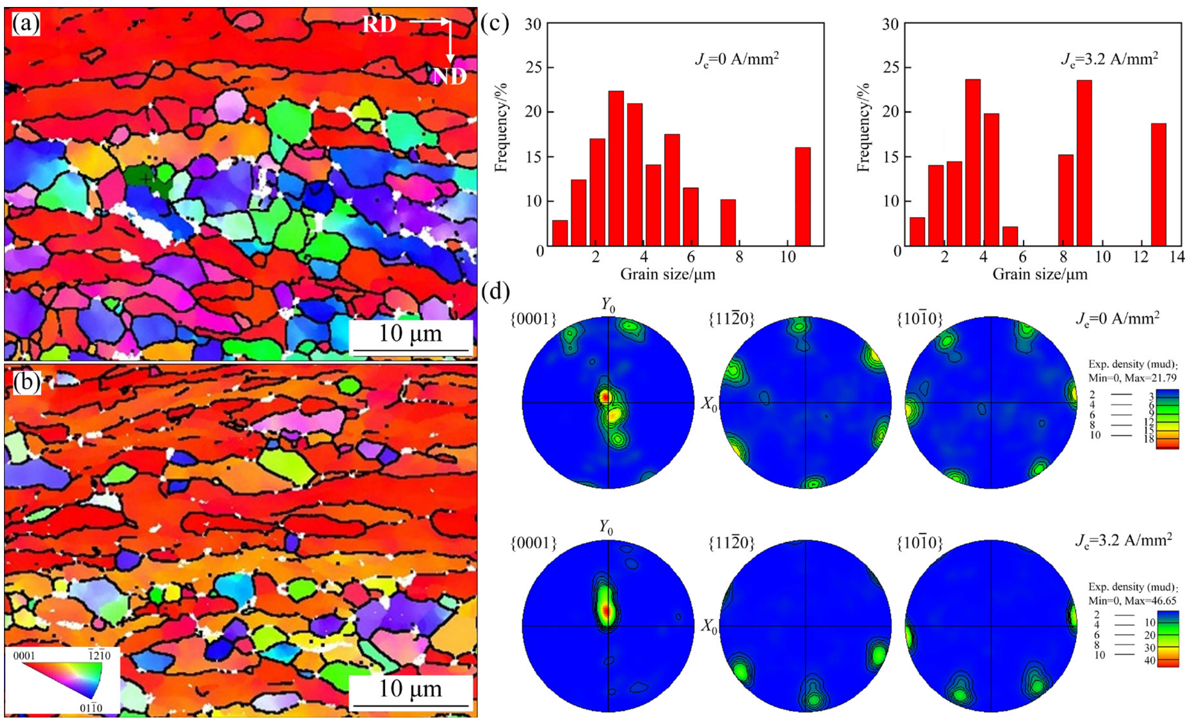

Fig. 6 Inverse pole figures at radius corner under current densities of 0 A/mm^2 (a) and 3.2 A/mm^2 (b), grain size distribution of α phase (c), and {0001}, {11$\bar{2}$0} and {10$\bar{1}$0} pole figures of α phase (d)

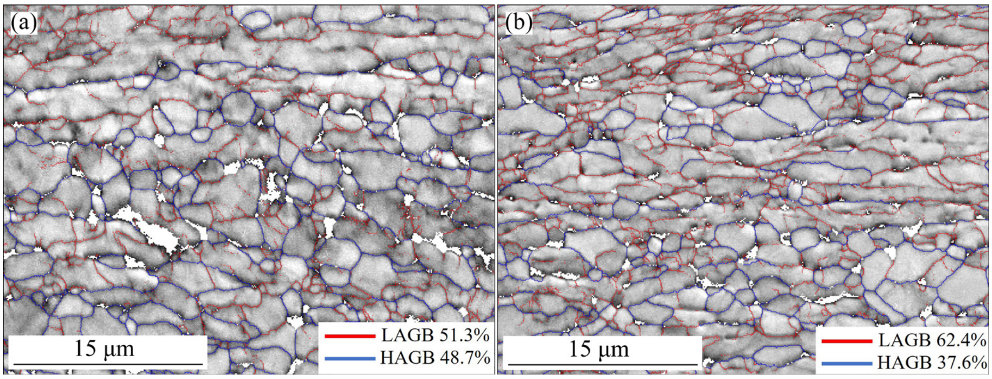

Fig. 7 Grain boundary distribution maps with greyscale of image quality at current densities of 0 A/mm^2 (a) and 3.2 A/mm^2 (b)

promoted dislocation rearrangement, leading to sub-grain structure formation [22]. In addition, the decreased HAGB fraction indicated that the recrystallization was not promoted under electropulsing of 3.2 A/mm^2.

The deformation mechanism under electropulsing was investigated by Schmid factor (SF) as shown in Fig. 8. The average SF values of basal $\langle a \rangle$, prismatic $\langle a \rangle$, and pyramidal $\langle c+a \rangle$ slip systems are listed in Table 2. The basal $\langle a \rangle$ slip system has the lowest SF value, implying the inhibition of slip activation during deformation. The prismatic $\langle a \rangle$ and pyramidal $\langle c+a \rangle$ slip systems are favorable to be activated due to large SF value. However, the $\langle c+a \rangle$ type slip system has large critical resolved shear stress (CRSS) value than $\langle a \rangle$ type slip system [23], thus the prismatic $\langle a \rangle$ slip contributes to deformation dominantly in present work. In addition, less prismatic $\langle a \rangle$ slip system is activated under electropulsing of 3.2 A/mm^2 than that of 0 A/mm^2, as shown in Table 2.

4 Discussion

4.1 Thermal effect of electropulsing

Electropulsing flows through alloy sheet and generates Joel heating effect, which can be divided into two parts as shown in Eq. (4):

$$\Phi_{\mathrm{J}}=\Delta\Phi_{\mathrm{S}}+\Delta\Phi_{\mathrm{Diss}} \tag{4}$$

where Φ_{J} is the Joel heating, Φ_{S} is the increased thermal energy in alloy sheet, and Φ_{Diss} is the thermal heat loss. In the initial stage of electropulsing-assisted bending, the thermal heat loss is limited due to the small temperature difference between the specimen and the environment ($\Phi_{\mathrm{J}}=\Delta\Phi_{\mathrm{S}}$). YANAGIMOTO and IZUMI [20], and ZHU et al [24] concluded that the temperature increase rate in this stage can be expressed by

$$\frac{\mathrm{d}T}{\mathrm{d}t}=\frac{R}{c\rho}\left(\frac{J_{\mathrm{e}}}{S}\right)^2 \tag{5}$$

where T is the temperature, t is the time, R is the electrical resistance of metal, c is the specific heat capacity, ρ is the density, and S is the cross-sectional area of the specimen. According to Eq. (5), the temperature increase rate is dependent on the square of effective current intensity. Therefore, the temperatures increase more rapidly in the initial stage under high current density in Fig. 3(d) and Fig. 5. After the initial stage, the thermal heat loss increases because of the large temperature difference between specimen and environment. The specimen reaches thermal stability when the thermal heat loss is equal to the increased thermal energy ($\Phi_{\mathrm{J}}=\Delta\Phi_{\mathrm{Diss}}$), where $\Delta\Phi_{\mathrm{Diss}}$ can be calculated as follows:

$$\Delta\Phi_{\mathrm{Diss}}=\left|\lambda A\frac{\mathrm{d}T}{\mathrm{d}t}\right|+hA'(T-T_0) \tag{6}$$

where T_0 is environmental temperature, A and A' are heat transfer areas between the specimen and the die, and between the specimen and the environment, respectively, λ is heat transfer coefficient, and h is convection heat transfer coefficient. Combining Eqs. (5) and (6), Eq. (7) can be obtained as follows:

$$\frac{\int J_{\mathrm{e}}^2(t)R\mathrm{d}t}{c\rho S^2}=\left|\lambda A\frac{\mathrm{d}T}{\mathrm{d}t}\right|+hA'(T-T_0) \tag{7}$$

The thermal stability temperature in present work thus can be calculated as

$$T=60.33J_{\mathrm{e}}^2+T_0 \tag{8}$$

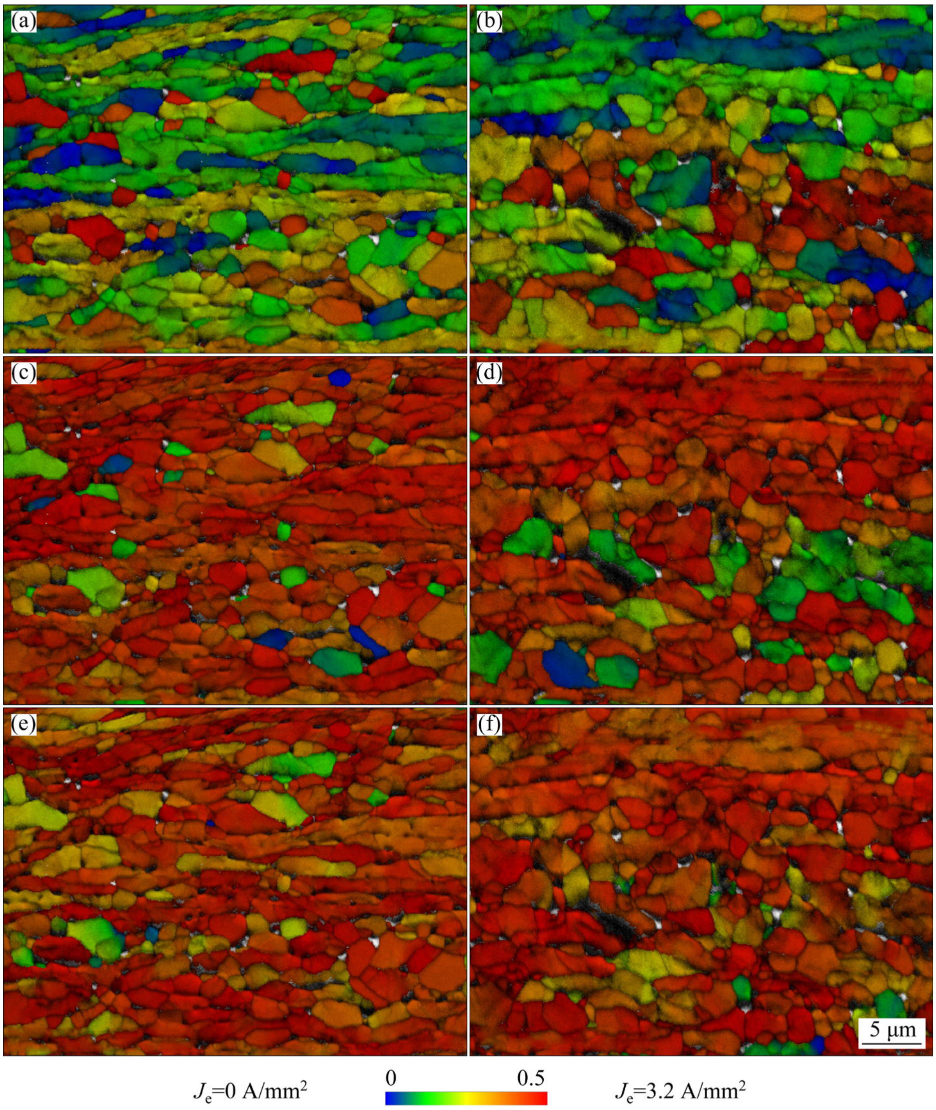

Fig. 8 Schmid factor maps of basal ⟨a⟩ (a, b), prismatic ⟨a⟩ (c, d), and pyramidal ⟨c+a⟩ (e, f) slip systems at current density of 0 A/mm^2 (a, c, e) and 3.2 A/mm^2 (b, d, f)

Table 2 Average Schmid factor values of basal ⟨a⟩, prismatic ⟨a⟩, and pyramidal ⟨c+a⟩ slip systems at different J_e values

J_e/ (A·mm^{-2})	Basal ⟨a⟩ {0001} ⟨$11\bar{2}0$⟩	Prismatic ⟨a⟩ {$10\bar{1}0$}⟨$11\bar{2}0$⟩	Pyramidal ⟨c+a⟩ {$10\bar{1}1$}⟨$11\bar{2}3$⟩
0	0.204	0.421	0.471
3.2	0.229	0.394	0.464

Therefore, the thermal stability temperature is dependent on the square of the effective current intensity. The higher current density causes higher thermal stability temperature. The calculated thermal stability temperatures by Eq. (8) together with the experimental temperatures are plotted in Fig. 9. It can be observed that the calculated and experimental curves overlap well with each other, indicating that Eq. (8) is reliable to predict temperature change during electropulsing-assisted bending in present work. The larger temperature deviation at high effective current density may be due to the increased thermal loss.

Thus, the electropulsing generated high temperature in a short time, softened alloy sheet and decreased the bending load value, which significantly improved the formability and suppressed springback. On the other hand, the electropulsing also determined microstructure and texture evolution during deformation. As shown in Section 3.4, {0001} basal texture was strengthened, and the activation of prismatic ⟨a⟩ slip system was

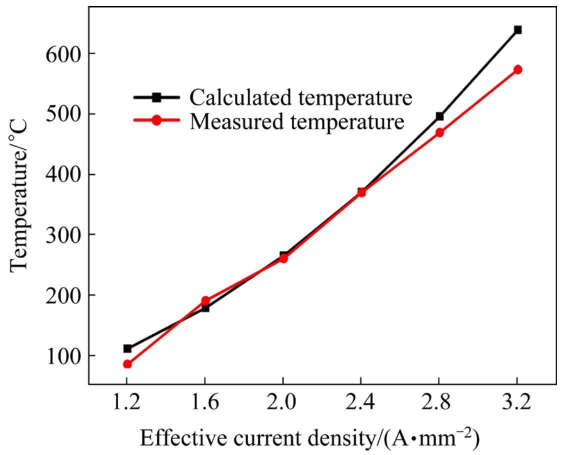

Fig. 9 Experimental and calculated thermal stability temperatures at different effective current densities

suppressed under electropulsing. It was reported that the strong {0001} texture led to high flow stress and low formability due to the slip system activation [8,25]. The {0001} orientated grains are unfavorable for prismatic ⟨*a*⟩ slip system activation because of the parallel or perpendicular relationship between prismatic $\{10\bar{1}0\}$ slip plane and force direction, therefore, the difficulty of prismatic ⟨*a*⟩ slip system activation increases the flow stress. However, in the present work, the strengthened {0001} texture under electropulsing did not increase flow stress because of the dramatical temperature increase. Besides, the suppressed prismatic ⟨*a*⟩ slip system may also contribute to the alloy softening. That is to say, the effect of {0001} texture strengthening on bending formability is limited under electropulsing due to temperature increase and slip system activation. In addition, electropulsing caused slight grain coarsening from 4.50 to 6.20 μm during bending. However, the formability deterioration by grain coarsening was not observed in the present work because the increased temperature by electropulsing led to outstanding alloy softening.

4.2 Athermal effect and microstructure evolution

The athermal effect of electropulsing in the present work is confirmed, as shown in Table 3. The thermal stability temperatures present a noticeable difference of more than 100 °C with different duty ratios at 3.2 A/mm^2, implying the unequal thermal effect of electropulsing. However, the bending angles of three specimens are almost same around 145°. The similar formability at different temperatures indicates that the athermal effect also contributes to formability improvement, especially at duty ratios of 10% and 70%. The dramatical athermal effect at duty ratios of 10% and 70% may be due to the high peak effective current density and long power-on time, respectively. It should be noted that, the reinforcement of athermal effect by adjusting electropulsing parameters can make low-temperature formability of Ti−6Al−4V alloy sheet comparable to that at higher temperature, which may avoid the grain coarsening and oxidation during hot forming.

Table 3 Thermal stability temperature and bending angle at various duty ratios and 3.2 A/mm^2

Duty ratio/%	Thermal stability temperature/°C	Bending angle/(°)
10	219	146.8
50	368	144.8
70	275	145.3

To discuss the dislocation density under electropulsing, the kernel average misorientation (KAM) maps and distribution curves are shown in Fig. 10. The bended specimen without electropulsing presents higher KAM value than the as-received sheet, indicating the higher dislocation density and dislocation accumulation after cold forming. However, the large dislocation accumulated area disappears after bending under 3.2 A/mm^2 (Fig. 10(c)). The KAM value curve shifts left compared with that of cold bending, indicating the decreased dislocation density. This is because pulse current can promote the dislocation motion, relieve dislocation pinning and decrease dislocation density by the electron wind effect. Electron wind effect accelerates interchange of vacancies and atoms through the increased driving pressure, therefore decreases dislocation density [26,27].

The LAGB and sub-grain formation is promoted by electropulsing, as discussed in Fig. 7. The LAGB formation mechanism is displayed through partial grain boundary map and KAM map in Fig. 11. As depicted in Figs. 11(a) and (c), the yellow arrow marks the *α* grain within high dislocation density and few LAGBs, this is because the dislocation is accumulated during cold bending. However, under electropulsing of 3.2 A/mm^2, the dislocation accumulation was relieved with lower

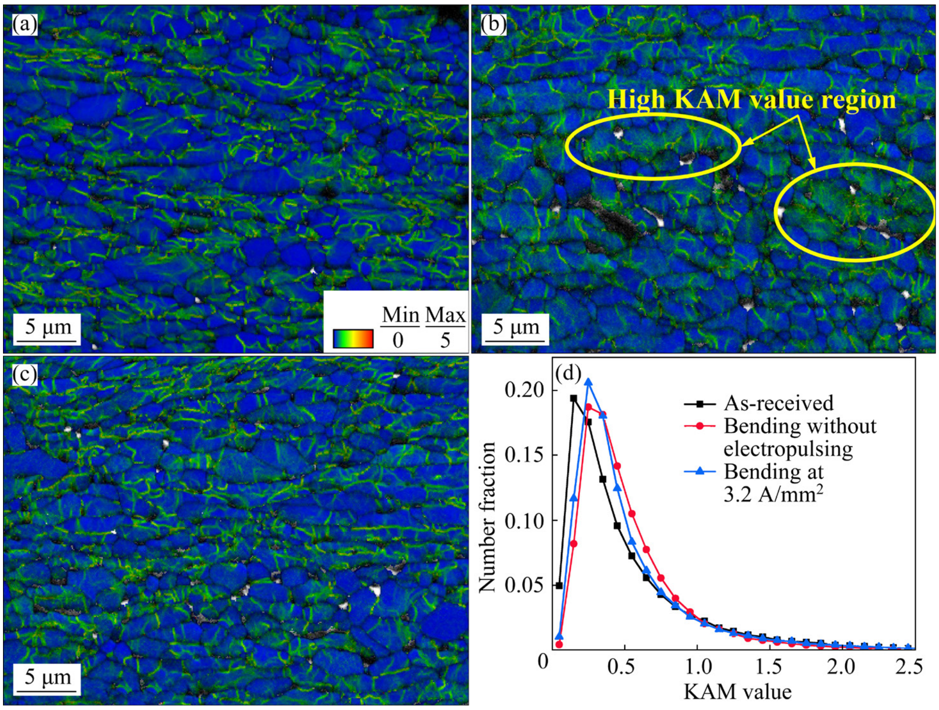

Fig. 10 KAM maps of as-received specimen (a), bended specimen without electropulsing (d), and bended specimen at 3.2 A/mm^2 (c) and KAM value distribution (d)

dislocation density and more LAGB formation (Figs. 11(b) and (d)). The formation process of the LAGB is explained as follows: the tangled dislocation broke up and relieved under electropulsing. Then, the dislocation migrated to the linear region and piled up there. The sub-grain boundary gradually formed with increasing piled-up dislocation [27]. As marked by yellow arrows, some LAGBs have already formed in the high dislocation density regions, whereas, some LAGBs are to be formed due to the insufficient piled-up dislocations. Such sub-grain formation released the accumulated dislocation inside α grains and made grain boundary migration and grain deformation easy [28−30]. It is noted that the recrystallization of α phase did not occur in the present work due to the insufficient temperature increase and deformation degree. Nonetheless, it is possible to obtain a recrystallized microstructure with refined grain size and weak texture by adjusting electropulsing and deformation parameters [13].

In conclusion, the athermal effect by electropulsing also plays an important role in the improvement of formability. The decreased dislocation density, the promoted dislocation motion and sub-grain formation contribute to the alloy softening.

5 Conclusions

(1) The forming limit increased and the crack changed to be shallow with increasing effective current density. The bending load and bending angle decreased as the effective current density increased. Duty ratios also determined bending angles under 3.2 A/mm^2, which were 146.8°, 135.0°, 144.8° and 145.3° at duty ratios of 10%, 30%, 50% and 70%, respectively.

(2) The thermal stability temperature increased with increasing effective current density, which was the main reason for formability improvement. The temperature varied non-monotonically with the change of duty ratio, where 30% duty ratio led to the highest temperature. The thermal stability temperature can be calculated as $T=60.33J_e^2+T_0$.

(3) Electropulsing caused grain coarsening, {0001} texture strengthening and sub-grain development during bending. Prismatic ⟨a⟩ slip system activated dominantly during bending, whereas, the basal ⟨a⟩ slip system was slightly promoted at 3.2 A/mm^2. However, the alloy hardening effect by {0001} texture was limited due to the dramatical temperature increase.

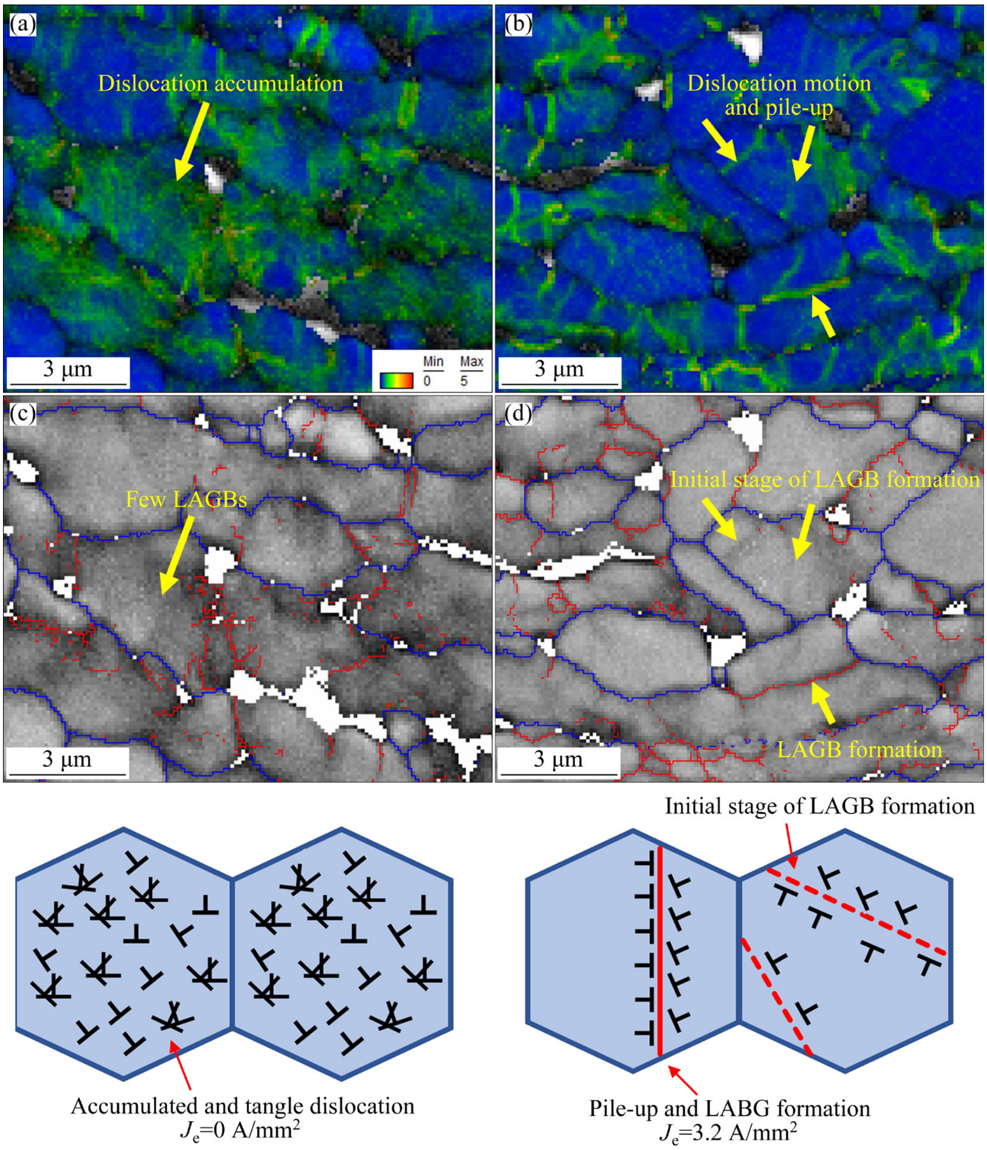

Fig. 11 KAM (a, b) and grain boundary (c, d) maps under electropulsing of 0 A/mm^2 (a, c) and 3.2 A/mm^2 (b, d)

(4) Thermal and athermal effects contributed to the formability improvement during electropusling-assisted bending. The thermal effect generated high temperature in a short time. The athermal effect decreased dislocation density, promoted sub-grain formation by dislocation motion and rearrangement.

CRediT authorship contribution statement

Ling-jian MENG: Conceptualization, Writing – Original draft, Methodology; **Hong-liang YIN:** Formal analysis, Methodology, Visualization; **Yan ZHU:** Formal analysis, Software, Experiment; **Xiao-lei CUI:** Investigation, Formal analysis, Review & editing; **Peng LIN:** Review & editing, Project administration, Funding acquisition.

Declaration of competing interest

The authors declare that they have no known competing financial interests or personal relationships that could have appeared to influence the work reported in this paper.

Acknowledgments

This work was supported by the National Natural Science Foundation of China (No. 51505323) and the Applied Basic Research Program of Shanxi Province, China (Nos. 20210302123117, 20210302124658).

References

[1] LÜTJERING G. Influence of processing on microstructure and mechanical properties of ($\alpha+\beta$) titanium alloys [J]. Materials Science and Engineering A, 1998, 243: 32−45.

[2] BANERJEE D, WILLIAMS J C. Perspectives on titanium science and technology [J]. Acta Materialia, 2013, 61: 844−879.

[3] ZHAN Mei, YANG He, GUO Jing, WANG Xian-xian. Review on hot spinning for difficult-to-deform lightweight metals [J]. Transactions of Nonferrous Metals Society of China, 2015, 25(6): 1732−1743.

[4] XU Wen-chen, SHAN De-bin, WANG Zeng-long, YANG Guo-ping, LÜ Yan, KANG Da-chang. Effect of spinning deformation on microstructure evolution and mechanical property of TA15 titanium alloy [J]. Transactions of Nonferrous Metals Society of China, 2007, 17(6): 1205−1211.

[5] WU Yong, FAN Rong-lei, QIN Zhong-huan, CHEN Ming-he. Shape controlling and property optimization of TA32 titanium alloy thin-walled part prepared by hot forming [J]. Transactions of Nonferrous Metals Society of China, 2021, 31(8): 2336−2357.

[6] ZONG Ying-ying, LIU Po, GUO Bin, SHAN De-bin. Springback evaluation in hot V-bending of Ti−6Al−4V alloy sheets [J]. The International Journal of Advanced Manufacturing Technology, 2015, 76: 577−585.

[7] LEI Zhen-ni, GAO Peng-fei, WANG Xian-xian, ZHAN Mei, LI Hong-wei. Analysis of anisotropy mechanism in the mechanical property of titanium alloy tube formed through hot flow forming [J]. Journal of Materials Science & Technology, 2021, 86: 77−90.

[8] FAN Rong-lei, WU Yong, CHEN Ming-he, XIE Lan-sheng. Relationship among microstructure, mechanical properties and texture of TA32 titanium alloy sheets during hot tensile deformation [J]. Transactions of Nonferrous Metals Society of China, 2020, 30(4): 928−943.

[9] WANG X X, ZHAN M, FU M W, GAO P F, GUO J, MA F. Microstructure evolution of Ti−6Al−2Zr−1Mo−1V alloy and its mechanism in multi-pass flow forming [J]. Journal of Materials Processing Technology, 2018, 261: 86−97.

[10] SHENG Yin-ying, HUA You-lu, WANG Xiao-jian, ZHAO Xue-yang, CHEN Lian-xi, ZHOU Han-yu, WANG J, BERNDT C C, LI Wei. Application of high-density electropulsing to improve the performance of metallic materials: Mechanisms, microstructure and properties [J]. Materials, 2018, 11(2): E185.

[11] AMBROGIO G, FILICE L, GAGLIARDI F. Formability of lightweight alloys by hot incremental sheet forming [J]. Materials & Design, 2012, 34: 501−508.

[12] AO Dong-wei, CHU Xing-rong, GAO Jun, YANG Yang, LIN Shu-xia. Experimental investigation on the deformation behaviors of Ti−6Al−4V sheet in electropulsing-assisted incremental forming [J]. The International Journal of Advanced Manufacturing Technology, 2019, 104: 4243−4254.

[13] SONG Hui, WANG Zhong-jin, GAO Tie-jun. Effect of high density electropulsing treatment on formability of TC4 titanium alloy sheet [J]. Transactions of Nonferrous Metals Society of China, 2007, 17(1): 87−92.

[14] XU Zhuo-hui, TANG Guo-yi, TIAN Shao-quan, DING Fei, TIAN Hao-yang. Research of electroplastic rolling of AZ31 Mg alloy strip [J]. Journal of Materials Processing Technology, 2007, 182(1/2/3): 128−133.

[15] OKAZAKI K, KAGAWA M, CONRAD H. An evaluation of the contributions of skin, pinch and heating effects to the electroplastic effect in titatnium [J]. Materials Science and Engineering, 1980, 45(2): 109−116.

[16] AO Dong-wei, CHU Xing-rong, YANG Yang, LIN Shu-xia, GAO Jun. Effect of electropulsing on springback during V-bending of Ti−6Al−4V titanium alloy sheet [J]. The International Journal of Advanced Manufacturing Technology, 2018, 96: 3197−3207.

[17] ZHAO Yi-xi, PENG Lin-fa, LAI Xin-min. Influence of the electric pulse on springback during stretch U-bending of Ti_6Al_4V titanium alloy sheets [J]. Journal of Materials Processing Technology, 2018, 261: 12−23.

[18] ZHOU Yan, CHEN Guo-qing, FU Xue-song, ZHOU Wen-long. Effect of electropulsing on deformation behavior of Ti−6Al−4V alloy during cold drawing [J]. Transactions of Nonferrous Metals Society of China, 2014, 24(4): 1012−1021.

[19] SONG Hui, WANG Zhong-jin. Microcrack healing and local recrystallization in pre-deformed sheet by high density electropulsing [J]. Materials Science and Engineering A, 2008, 490(1/2): 1−6.

[20] YANAGIMOTO J, IZUMI R. Continuous electric resistance heating: Hot forming system for high-alloy metals with poor workability [J]. Journal of Materials Processing Technology, 2009, 209: 3060−3068.

[21] LEI Lei, ZHAO Qin-yang, WU Cong, ZHAO Yong-qing, HUANG Shi-xing, JIA Wei-ju, ZENG Wei-dong. Variant selection, coarsening behavior of α phase and associated tensile properties in an $\alpha+\beta$ titanium alloy [J]. Journal of Materials Science & Technology, 2022, 99: 101−113.

[22] BAO Jian-xing, XU Jie, BAI Jia-nan, LV Shou-dan, SHAN De-bin, GUO Bin. Mechanical behavior and shear banding of electropulsing-assisted micro-scale shear−compression in Ti−6Al−4V alloy [J]. Materials Science and Engineering A, 2020, 771: 138647.

[23] ZAEFFERER S. A study of active deformation systems in titanium alloys: Dependence on alloy composition and correlation with deformation texture [J]. Materials Science and Engineering A, 2003, 344(1/2): 20−30.

[24] ZHU R F, TANG G Y, SHI S Q, FU M W. Microstructure evolution of copper strips with gradient temperature in electropulsing treatment [J]. Journal of Alloys and Compounds, 2013, 581: 160−165.

[25] IWANAGA K, TASHIRO H, OKAMOTO H, SHIMIZU K. Improvement of formability from room temperature to warm temperature in AZ-31 magnesium alloy [J]. Journal of Materials Processing Technology, 2004, 155/156: 1313−1316.

[26] LI Da-long, YU En-lin, LIU Zhou-tong. Microscopic mechanism and numerical calculation of electroplastic effect on metal's flow stress [J]. Materials Science and Engineering A, 2013, 580: 410−413.

[27] SONG Hui, WANG Zhong-jin. Effect of electropulsing on dislocation mobility of titanium sheet [J]. Transactions of Nonferrous Metals Society of China, 2012, 22(7): 1599−1605.

[28] ZHU Ru-fei, JIANG Yan-bin, GUAN Lei, LI Huai-lin,

TANG Guo-yi. Difference in recrystallization between electropulsing-treated and furnace-treated NiTi alloy [J]. Journal of Alloys and Compounds, 2016, 658: 548−554.

[29] LI He-zong, DONG Xiang-huai, SHEN Yu, DIEHL A, HAGENAH H, ENGEL U, MERKLEIN M. Size effect on springback behavior due to plastic strain gradient hardening in microbending process of pure aluminum foils [J]. Materials Science and Engineering A, 2010, 527(16/17): 4497−4504.

[30] FAKHAR N, SABBAGHIAN M. Hot shear deformation constitutive analysis of fine-grained ZK60 Mg alloy sheet fabricated via dual equal channel lateral extrusion and sheet extrusion [J]. Transactions of Nonferrous Metals Society of China, 2022, 32(8): 2541−2556.

Ti−6Al−4V 合金板材在电脉冲辅助弯曲过程中的显微组织演变及成形性能

孟令健[1]，殷宏亮[1]，朱 岩[1]，崔晓磊[2]，林 鹏[1,3]

1. 太原理工大学 材料科学与工程学院，太原 030024；
2. 哈尔滨工业大学 金属精密热加工国家重点实验室，哈尔滨 150001；
3. 太原理工大学 先进金属复合材料成形技术与装备教育部工程研究中心，太原 030024

摘 要：在有效电流密度为 0~3.2 A/mm^2、占空比为 10%~70%条件下对 Ti−6Al−4V 合金板材进行电脉冲辅助弯曲实验。结果表明：当有效电流密度从 0 增加到 2.4 A/mm^2 时，弯曲成形位移从 9.15 mm 增加到 15.60 mm；同时，裂纹的尺寸和宽度减小。此外，当弯曲位移为 8 mm 时，回弹角随着有效电流密度的增加而减小。占空比同样影响弯曲角，在 30%占空比条件下能获得最小的弯曲角 135.0°。板材的热稳定温度随着有效电流密度的增加而增加，但是与占空比呈非线性关系。此外，在电脉冲辅助弯曲过程中出现了晶粒粗化、{0001}织构强度增加和亚晶粒发展。电脉冲使位错密度降低且加速位错的重排，促进 α 晶粒内亚晶粒的形成，从而改善合金的成形性。电脉冲的非热效应提高了 Ti−6Al−4V 合金板材的低温成形性，使其与高温下的成形效果类似。

关键词：Ti−6Al−4V 合金板材；显微组织演变；成形性；电脉冲辅助弯曲；回弹；位错；非热效应

(Edited by Wei-ping CHEN)